Effectiveness of Carbonic Anhydrase Inhibitor Loaded Nanoparticles in the Treatment of Diabetic Retinopathy

Nagihan Uğurlu (drnahiganu@gmail.com)
Ankara Yıldırım Beyazıt University, Advanced Technologies Application and Research Center
Ebru Erdal
Ankara Yıldırım Beyazıt University, Advanced Technologies Application and Research Center
Soheil Malekghasemi
Hacettepe University
Murat Demirbilek
Ankara Haci Bayram Veli University

Research Article

Keywords: Diabetic retinopathy, Nanoparticles, Poly(3-hydroxybutyrate-co-3-hydroxyvalerate), Carbonic anhydrase inhibitor, Acetazolamide

Posted Date: May 24th, 2022

DOI: https://doi.org/10.21203/rs.3.rs-1666164/v1

Abstract

DRP is a disease consisting of all the structural and functional changes that develop in the retinal layer of the eye due to diabetes. DRP is the most important cause of blindness between the ages of 20-74 in the world, and the most successful standard treatment option in the treatment of DRP is intravitreal injections. To synthesize acetazolamide loaded nanoparticles to be applied intravitreal treatment of DRP and to examine the *in vitro* efficacy of the nanoparticles. ACZ loaded PHBV nanoparticles (PHBV-ACZ NPs) formulations were prepared. Nanoparticles with a particle size of 253.20±0.55nm. A DRP model was established and characterized in HRMEC cells. The effect of the nanoparticles on permeability has been investigated and carrier proteins in BRB due to the development of DRP has been investigated. To establish the *in vitro* DRP model, HRMEC was stimulated with Recombinant human 165 Vascular Endothelial Growth Factor (VEGF), thereby temporarily reducing the expression levels of endothelial junction proteins, increasing the number of intercellular spaces in the monolayers of HRMECs. It was determined that after the cells were exposed to Carbonic anhydrase inhibitors (CAI) loaded nanoparticles, permeability decreased and protein expression increased.

1. Introduction

Diabetic Retinopathy (DRP) is a clinical process formed by all structural and functional changes in the retinal layer of the eye due to Diabetes Mellitus. The retinal layer is vital for vision, so the damage to the retinal tissue due to diabetes causes decreased vision and blindness. DRP is the most important cause of blindness between the ages of 20–74 (CDC 2018). Approximately 4.2 million people in the world experience severe vision loss due to DRP [1]. Two main pathologies that cause vision loss in DRP pathogenesis are retinal neovascularization and increased retinal vascular permeability. While the development of neovascular tissues in the optic disc surface and retina due to the progressive deterioration of retinal perfusion leads to the development of Proliferative Diabetic Retinopathy, fluid accumulation in the between retinal layers or macular region due to diabetes is also defined as Diabetic macular edema (DME). While pan retinal photocoagulation is the best standard treatment in DRP treatment, macular edema is the first option intravitreal administered pharmacological agents [2].

The most important strategy in preventing DRP related blindness is the effective treatment of DRP indications. Intravitreal applications provide significant improvement in both anatomical and visual levels [3, 4]. Besides their high efficiency, intravitreal treatments used in DME treatment have serious limitations [5]. These limitations lead to intravitreal treatments not being applied at the targeted level in clinical practice. The results reported from long-term follow-up data of intravitreal injection therapy in DME and other posterior segment diseases are very different from prospective controlled randomized studies [6]. The visual enhancement levels obtained from the patients are much lower than the levels reported in controlled randomized studies [7–9].

One of the most important challenges in the treatment of retinal diseases is the difficulty of effective drug delivery (drug delivery) to the posterior segment due to the unique anatomical and physiological barriers of the eye [10, 11]. In the treatment of posterior segment diseases such as DRP, the most effective route of administration to provide an effective dose in the vitreous is intravitreal injections [12–14]. When the drug molecules are applied to the eye by intravitreal application without any carrier, they are rapidly removed from the vitreous. Therefore, repeated intravitreal injection applications are required to achieve the desired intravitreal drug concentration. Repeated intravitreal applications both lead to high costs and increase the risk of serious complications such as retinal detachment and endophthalmitis [15].

DRP is a chronic disease that requires long-term treatment. For this reason, new, non-toxic, biocompatible drug delivery systems that will extend the retention time of the drug in the vitreous are needed to prevent complications that may develop due to repeated intravitreal injections.

In the last decade, many studies have been conducted on drug delivery of nanoparticular drug delivery systems to the posterior segment and their use in many other biomedical fields [10, 16]. Intravitreal nanoparticular drug delivery systems provide advantages such as allowing the administration of drugs with high efficiency but low solubility and low half-life, reducing the frequency of intravitreal injection by providing controlled release and increasing the treatment response by increasing the transition to retinal tissue [10, 13, 15, 17].

Polyhydroxyalkonates (PHA), which is a member of the polyester family and are macromolecules where prokaryotes store energy, are biodegradable and biocompatible biomaterials that are widely preferred in the development of drug delivery systems [18, 19].

Due to their production by natural resources, thermoplasticity, biocompatibility and biodegradability, PHAs are materials that have a wide application area for many sectors, especially the biomedical sector [20, 21]. Poly(3-hydroxybutyrate-co-3-hydroxyvalerate) (PHBV) is a linear structured aliphatic polyester belonging to the PHA family [22]. PHBV is a copolymer of hydroxybutyrate (HB) and hydroxyvalerate (HV) at different molar concentrations. PHBV's mechanical properties can be modified and 3 hydroxybutyric acid, which is a degradation product, is a metabolite that can be found in human blood [23]. Nanoparticular drug delivery systems developed for eye application should also be biocompatible, non-toxic and biodegradable [24]. For this reason, PHBV is widely used in nanoparticular systems developed for the eye [25–28].

Intravitreal anti-VEGF effective drugs are effective treatment methods that provide both anatomical improvement and a significant increase in vision level in DME treatment. However, 30–50% patients do not respond to treatment [29–33]. It is thought that structural changes in the retina or pathways independent of VEGF may also be effective in this nonresponse [34–39]. Therefore, the use of combined therapies in refractory DME treatment is a preferred option [12, 40].

The pilot study showed the result that the administration of acetazolamide is effective in the treatment of diabetic retinopathy of Acetazolamide (ACZ). ACZ is a drug with low solubility and a very short half-life, and its low bioavailability necessitates its systemic administration. As a result, serious side effects may develop. For these reasons, ACZ is administered orally for short time only before surgery or in emergency situations in the treatment of eye diseases [41]. Although ACZ has high efficacy, its use for the treatment of macular edema is limited due to its low bioavailability. Dexamethasone is an active substance that has been shown to be effective in the treatment of DME [42]. Within the scope of the presented study, it is aimed to develop a drug delivery system that will allow the combined administration of ACZ and dexamethasone (steroid) active ingredients.

2. Materials And Methods

2.1. Chemicals

Poly (3-hydroxybutyrate-co-3-hydroxy valerate) (PHBV), Polyvinyl alcohol (PVA) used in the preparation of nanoparticles, and dexamethasone the active substance Acetazolamide (ACZ) loaded into the particles were supplied from Sigma. Dichloromethane and ammonium were used as solvents and purchased from Carlo Erba. The WST-1 assay, used for the toxicity test, was obtained from Intron Biotechnology. Complete cell medium, serum, and antibiotic used in the culture of human retinal microvascular endothelial cell line (HRMEC) supplied from Cell System and Corning, respectively. ELISA kits purchased from CK Biotech were used for cell-based ELISA studies to measure carrier proteins and intercellular connection structures. TNF alpha and IL10 levels were determined by using ELISA kits from Cloud-Clone Corp.

2.2. Preparation of ACZ-PHBV NPs

Acetazolamide loaded PHBV nanoparticles (PHBV-ACZ NP) were prepared by modified double emulsification (w1/O1/w2) solvent-evaporation technique [43]. Briefly, PHBV polymeric solution dissolved in dichloromethane were prepared as organic phase in different concentrations (0.3-2% w/v). ACZ solution, dissolved in 1 M NH_4OH at concentrations between 0.1 and 1% w/v, was added dropwise to the polymeric solution and sonicated for 180 s at a power output of 150 W using an ultrasonic homogenizer (Model: HD4200, Bandelin) to obtain the first emulsion (w1/O). The w1/O emulsion was then mixed with aqueous solution of 0.1–1.5% w/v PVA (w2) and further emulsified by sonication under the same conditions. Afterward, the w1/O1/w2 emulsion was immediately poured into 0.5% w/v PVA solution and the resulting emulsion was stirred at 900 rpm for 6 h to allow complete evaporation of the organic solvent. The resultant dispersion was centrifuged (Eppendorf, 5804R, Germany) at 11.000 rpm for 20 min. The supernatant was then stored to determine the concentration of ACZ loaded into the nanoparticles and the pellet was washed three times with deionized water. The collected PHBV-ACZ NPs were resuspended in phosphate buffered saline (PBS) and stored at + 4°C for further use. The same method was used to prepare bare PHBV NP, except that deionized water was added instead of ACZ solution.

Experimental design and systematic optimization

The Box–Behnken design plays an important role in statistical modeling as it is the most cost-effective and requires less experimental runs for optimization. The systematic optimization of PHBV-ACZ NPs was conducted using Box-Behnken design (BBD), one of the most used response surface method (RSM) (Design Expert® ver. 9.0 software, Stat-Ease Inc., Minneapolis, USA).

In the present study, three most influential independent variables including concentration of PHBV (X1), PVA (X2), and ACZ (X3) were selected for optimization at three different levels coded as high level (+ 1), medium level (0) and low level (-1) (Table 1) [44, 45]. Physicochemical properties including nanoparticle size (nm) (Y1), polydispersity index (PDI) (Y2), and entrapment Efficiency (%) (Y3) of prepared PHBV-ACZ NPs were analyzed as responses (dependent variables). The software as shown in Table 2 suggested a total of 17 runs.

Table 1
Variables used in Box-Behnken experimental design

	Levels		
Independent Variables	Low (-1)	Medium (0)	High (+ 1)
PHBV Concentration (% w/v)	0.3	1.15	2
PVA Concentration (% w/v)	0.1	0.8	1.5
Drug Concentration (% w/v)	0.1	0.55	1
Dependent Variables	**Physicochemical properties**		
Nanoparticle Size (nm)	-	-	-
Polydispersity Index (PDI)	-	-	-
Entrapment Efficiency (%)	-	-	-

Table 2
Experimental design and related responses in various trials with Box-Behnken software

	Independent variables			Dependent variables (Average ± SD)		
Trial	PHBV Cons. (% w/v)	PVA Cons. (% w/v)	ACZ Cons. (% w/v)	Nanoparticle size (nm)	Polydisperrsity Index (PDI)	Entrapment Efficiency (%)
1	0.3	0.8	0.1	330 ± 4	0.115 ± 0.024	64 ± 2.58
2	1.15	0.1	1	251 ± 3.7	0.069 ± 0.031	66.29 ± 2.37
3	2	1.5	0.55	250.9 ± 7.4	0.05 ± 0.038	49.05 ± 2.95
4	0.3	0.8	1	314.3 ± 6.3	0.112 ± 0.04	50.07 ± 2.13
5	1.15	0.8	0.55	283.5 ± 4.98	0.083 ± 0.03	50 ± 3.01
6	2	0.8	0.1	306.2 ± 8.38	0.12 ± 0.013	71.71 ± 2.98
7	2	0.1	0.55	364.8 ± 0.93	0.254 ± 0.013	44.81 ± 3.32
8	1.15	0.8	0.55	303.7 ± 3.017	0.06 ± 0.016	46 ± 3.76
9	1.15	1.5	0.1	290.9 ± 7.23	0.098 ± 0.02	67.92 ± 3.93
10	1.15	0.1	0.1	356.2 ± 9.63	0.146 ± 0.02	64.65 ± 3.51
11	1.15	1.5	1	278.7 ± 3.83	0.049 ± 0.023	45.11 ± 2.10
12	2	0.8	1	276 ± 5.42	0.037 ± 0.014	47.71 ± 3.87
13	1.15	0.8	0.55	287.8 ± 6.15	0.062 ± 0.035	49.26 ± 3.55
14	1.15	0.8	0.55	293.1 ± 3.651	0.036 ± 0.038	45 ± 2.78
15	0.3	0.1	0.55	362.5 ± 8.947	0.167 ± 0.039	43 ± 2.74
16	1.15	0.8	0.55	306.5 ± 0.173	0.091 ± 0.01	41.18 ± 3.86
17	0.3	1.5	0.55	342 ± 5.359	0.074 ± 0.049	49.41 ± 2.61

Table 1. Variables used in Box-Behnken experimental design

Table 1 *is attached*

Based on the Design-Expert software, 12 of 17 experimental trials were obtained from a combination of boundary and midpoint of the process area, and the other five were obtained only from the center point. In this study, all experimental trials were conducted in triplicate to minimize error and maintain precision. The impact of dependent and independent variables is modeled by the following polynomial equation in terms of linear, quadratic and cross-product terms:

$$Y = \beta_0 + \beta_1 X_1 + \beta_2 X_2 + \beta_3 X_3 + \beta_{12} X_1 X_2 + \beta_{13} X_1 X_3 + \beta_{23} X_2 X_3 + \beta_{11} X_1^2 + \beta_{22} X_2^2 + \beta_{33} X_3^2$$

Where, Y is the predicted response, β_0 is intercept, X1, X2, and X3 are factors (independent variables), β1, β2, and β3, represents linear coefficients, β11, β22, and β33 represents quadratic coefficients and β12, β13 and β23 represents interaction coefficients [46]. Multiple linear regression or data fitting with the quadratic polynomial model was analyzed by ANOVA to determine the significance and influence of parameters on dependent variables (responses). The adequacy of the quadratic polynomial model was evaluated with the coefficient of correlation (r2), F-value, and lack of fit value. 3D surface plots were generated to graphically identify the interaction and relationship between parameters and dependent variables. Optimizations were also performed using numerical desirability functions to understand the values of the independent variables in which PHBV-ACZ NP with appropriate physicochemical properties is synthesized.

Table 2. Experimental design and related responses in various trials with Box-Behnken software

Table 2 *is attached*

2.3. Determination of size, size distributions and zeta potentials of nanoparticles

The size, polydispersity index, and zeta potential (ζ-potential) of the nanoparticles were determined by Zeta Sizer (Malvern Instruments, Model 3000 HSA, Malvern, UK). The nanoparticles were diluted (1:10 v/v) appropriately with ultra-pure water and after they were placed in the corresponding cuvette, measurements were made at 25°C. All measurements were made in triplicate. The zeta potential of the prepared NPs was calculated from the electrophoretic mobility using the Helmholtz-Smoluchowski equation. To avoid multiple scattering effects, dilution was also made in ultra-pure water before analysis.

Surface morphology characterization of synthesized nanoparticles was evaluated using focused ion beam scanning electron microscopy (FIB-SEM, TESCAN, GAIA 3). Before scanning, PHBV-ACZ NP samples were dropped onto carbon banded aluminum stubs and then coated with a 5-nm thick gold/palladium alloy under argon pressure.

2.4. Determination of ACZ release profiles and loading rates of nanoparticles

The indirect method was carried out to determine the entrapment efficiency (EE) of the loaded drug. In the indirect method, the percentage of encapsulated ACZ was calculated by subtracting the initial amount of ACZ from the unloaded ACZ remaining in the aqueous medium during washing and supernatant. The loading efficiency (LE%) was calculated by dividing the total weight of ACZ entrapped in the nanoparticles by the total nanoparticle weight. In drug delivery, the percent yield is a reflection of the amount of drug delivered per the amount encapsulated. These calculations were made according to the following equation:

$$\mathrm{EE\%} = \frac{\mathrm{initialACZ} - \mathrm{unloadedACZ}}{\mathrm{initialACZ}} \times 100$$

$$\mathrm{LE\%} = \frac{\mathrm{amountoftotalentrappedACZ}}{\mathrm{totalnanoparticleweight}} \times 100$$

Before starting the drug release study, the dialysis membrane (cut-off 14 – 12 kDa, Sigma) was soaked in diffusion medium-PBS (phosphate buffer solution, pH 7.4) overnight. Nanoparticles homogeneously distributed in PBS were placed on the dialysis membrane at 5.5 mg/ml and then both ends of the membrane were closed. The dialysis membrane was placed in the recipient chamber containing 50 ml of PBS and the system was incubated at 37 ± 1^{O}C with stirring at 50 rpm. To prevent the solution in the receiver compartment from evaporating, the compartment is covered with a cover. Samples were taken at regular time intervals (0, 15, 30, 60, 120, 180, 240, 300, 360, 420, and 480 minutes) and a fresh medium was added to the receiver compartment for the same volume. Samples were analyzed using a UV spectrophotometer at 293nm. All experiments were repeated 3 times and average values were taken.

2.5. Determining the stability/degradation time of nanoparticles

The degradation rate of PHBV-ACZ NP was measured with a turbidimeter device (Lovibond, TB 300 IR). 0.48 mg/mL PHBV-ACZ NP (n = 3) were suspended in PBS and incubated at different temperatures (4°C and 37°C) for 4 weeks. The turbidimetric absorbances of the samples were recorded weekly. One of the important aspects affecting the drug release profile is the rate of degradation of nanoparticles [47]. All measurements were repeated 3 times and average values were taken.

2.6. *In vitro* efficacy of nanoparticles

To determine the *in vitro* efficiency of nanoparticles of different formulations and concentrations; cytotoxicity, hemocompatibility, permeability and changes in cell surface carrier proteins of nanoparticles were investigated. Within the scope of the study, a drug delivery system has been developed that will allow the combined administration of both ACZ and dexamethasone (steroid) active ingredients. In practice, it is aimed that dexamethasone will act first, and then ACZ will continue this effect with controlled release from nanoparticles. To obtain PHBV-ACZ-St NP; ACZ-loaded PHBV NPs were suspended with dexamethasone solution (0.125mg/100 mL) and used. Active ingredients (ACZ and steroid) used with empty PHBV NP, PHBV-ACZ NP and PHBV-ACZ-St NP were also evaluated in *in vitro* studies.

2.6.1. Determination of the cytotoxicity of nanoparticles on HRMEC and human monocyte/macrophage cell line (THP-1)

In the study, the cytotoxicity of nanoparticles and ACZ in different concentrations and formulations was determined by the WST-1 test. For this; the toxicity of blank PHBV nanoparticles, acetazolamide loaded PHBV nanoparticles, acetazolamide loaded and steroid coated PHBV nanoparticles, steroid, and ACZ on the human retinal microvascular endothelial cell line (HRMEC) were determined. Concentrations of 1, 10, 50, 100 and 250 µg/ml were determined to determine the effect of formulations with different concentrations.

HRMEC cell line was cultured with complete cell medium (Cell System) containing serum and antibiotics specific for eye endothelial cells. HRMEC were seeded at a concentration of 5000 cells/well into 96-well plates and the plates were incubated in a $37^{O}C$, 5% CO_2 incubator. The sterilization of the nanoparticles was done with 0.45µm diameter injector filters. The nanoparticle solution was sterilized by UV for 20 minutes after filtering. The next day, the medium in the wells was replaced with media containing nanoparticle formulations at concentrations of 1, 10, 50, 100 and 250 µg/ml. After the cells were incubated with nanoparticles for 24 hours, the medium was removed and 200µl of WST-1 reagent was added to each well. After 2 hours of incubation, the plate was read at 440nm.

For the determination of the cytotoxicity of nanoparticles in the THP-1 cell line, firstly, PMA (Phorbol 12-myristate 13-acetate) was dissolved in the cell medium at a concentration of 100nM/ml. THP-1 cells (5000 cells/ml) were seeded into 24-well plates with a medium containing PMA and the plates were incubated in a $37^{O}C$, 5% CO_2 incubator. THP-1 cells were checked at regular intervals and their transformation into macrophages was visualized. After the cells were transformed into macrophages, nanoparticles in different formulations, ACZ and steroids were prepared at concentrations of 1, 10, 50, 100 and 250 µg/ml. Particles were added to the cells and incubated for 48 hours in $37^{O}C$, 5% CO_2 incubator. After 48 hours of incubation, media were taken and cytotoxicity was determined by WST-1 test.

2.6.2. Determination of the effect of nanoparticles on cytokine response using THP-1 cell line

Macrophages are considered to be the cells that first come into contact with the invading pathogen and initiate the natural immune/inflammatory response. Inflammation is the immune system's first response to infection or irritation regulated by cytokines. While pro-inflammatory cytokines such as IL-1, IL-6, IL-8, and TNF alpha provide activation of inflammatory cells; anti-inflammatory cytokines such as IL-10 prevent excessive tissue damage. Therefore, there is a balance between cytokine types [48]. The cytokine response of the nanoparticles and its comparison with the cytotoxic effect is critical for the application of the materials.

After the cells were transformed into macrophages, test materials were added to the cells and incubated at $37^{O}C$, 5% CO_2 for 48 hours. After 48 hours of incubation, the media were taken and after centrifugation at 2500 rpm for 5 minutes, TNF alpha and IL10 levels in the medium were measured with commercial kits.

2.6.3. Hemocompatibility of nanoparticles

Hemocompatibility is defined as the compatibility of blood substances and materials. Generally, materials intended for *in vivo* administration interact with at least one of the many compounds found in the blood. Therefore, it is necessary to determine the hemolytic effects of the materials developed as a result of their interaction with blood [49]. In the study, the rate of nanoparticles to hemolyzed erythrocytes was determined. In this context; nanoparticles with different formulations, steroid, and ACZ were prepared at concentrations of 1, 10, 50, 100 and 250 µg/ml. Rabbit blood taken into EDTA tubes was diluted 1/10 with PBS. The materials interacted with blood for 1 hour at $37^{O}C$. Then, the samples were centrifuged at 1500 rpm for 5 minutes and the plasma parts were measured at 540nm. PBS was used as negative control and purified water as a positive control.

2.6.4. Creation of DRP model in HRMEC Culture

The human retinal microvascular endothelial cell line (HRMEC) was cultured with a complete cell medium (Cell System) containing serum and antibiotics. After the flask surface was coated with an attachment factor that allows the cells to adhere to the surface,

the cells were added to the medium and incubated at 37^{O}C, 5% CO_2, and 95% relative moisture.

In the literature, cells are interacted with VEGF to create a diabetic retinopathy model in the HRMEC [50]. Studies have been carried using different concentrations of VEGF. In our research, the most effective result was obtained with a medium containing VEGF at a concentration of 150ng/ml, and this concentration was used in ongoing studies.

2.6.5. TEER Testing in all nanoparticle's groups and comparison of data

Transepithelial/endothelial electrical resistance (TEER) is a non-invasive method used for the evaluation of cellular connections and integrity in cell lines with barrier functions such as endothelial cells. The cell confluence made up of a single layer (monolayer) can be analyzed by TEER measurement. As the intercellular spaces are closed, there is a gradual increase in TEER measurement. As the barrier function is impaired in the DRP cell culture model, the resistance values obtained as a result of TEER measurements decrease compared to normal values [51]. Within the scope of the study, the differences in the resistance values were compared by measuring the TEER measurement results in the control, VEGF, and VEGF-nanoparticle groups. 3 inserts were seeded for each group.

Each stage of TEER measurements and permeability tests were performed using a complete cell medium. For this, a system with two compartments is used. For this, an insert consisting of a polycarbonate membrane with a pore diameter of 0.4µm was placed in a 12-well plate. HRMEC cells were added after the insert surface was coated with an attachment factor. 24 hours after the cells were seeded, TEER values were measured and whether the cells covered the insert surface or not was determined by the TEER values obtained [52].

2.6.6. Permeability Analysis

In permeability analysis, as in TEER measurements, a system with 2 compartments was used. Cells were incubated for 24 hours with VEGF-containing media after covering the insert surface. At the end of this period, the cells were exposed to nanoparticles. In the study were determined 3 groups (Control, VEGF, and VEGF-nanoparticle groups). The control group interacted with only cell culture medium, the VEGF group with 150ng/ml VEGF, and the VEGF-nanoparticle group with 150ng/ml VEGF and nanoparticles at a certain concentration. After 48 h incubation with the nanoparticle, a permeability test was performed. The medium in the upper compartment was replaced with the same volume medium containing 70 kDa FITC conjugated dextran (500µg/ml). After 2 hours of incubation, the medium in the lower chamber was removed and the concentrations of the dextran were determined using a fluorescence reader at 528nm emission/485nm excitation wavelength. Concentrations were calculated comparatively and passage through cell-free wells was taken as control.

2.6.7. Cell Based ELISA Tests

Carrier proteins on the cell surface and intercellular connection structures form the structure of the blood-retinal barrier. In the development of *in vitro* and *in vivo* DRP model, damage occurs on the cell surface of the blood-retinal barrier and occurs at the level of proteins [51]. In the study, the quantities of VE-Cad, ZO-1, PLVAP, Cav-1, laminin, Claudin 5 proteins in cell lines were determined using commercial kits by the ELISA method. In the first step, HRMECs were seeded with 25T flasks. After it was determined that the cells covered 90% off the plate surface, 1 flask was left as the control group and incubated with medium at 37^{O}C, 5% CO_2. VEGF-containing medium was added to the other flasks and incubated for 48 hours. At the end of 48 hours, nanoparticles of different formulations, steroids, and ACZ were added to the wells. After 48 h incubation, cells were washed with cold PBS and lysed in PBS. Samples obtained from each flask were kept at -80^{O}C for ELISA test measurements.

3. Results And Discussion

3.1. Optimization of PHBV-ACZ NP

Optimization process of nanoparticle synthesis was carried out using BBD. Table 3 shows the responses of the 17 trials proposed by the BBD. In this study, BBD was performed to obtain optimum levels of polymer (X1), surfactant (X2), and drug (X3) concentration as independent variables. These independent variables were affected nanoparticle size (Y1), size distribution (Y2), and entrapment efficiency of active ingredient (Y3), which are known as critical parameters for nanoparticulate drug delivery system.

Table 3
Observed levels, constraints and prediction errors of dependent variables in Box-Behnken design.

Dependent variables		Restriction	Predicted value	Experimental value**	Prediction error (%)
Y_1 = Nanoparticle size (nm)		Minimize	254.46	253.20 ± 0.55	-0.5
Y_2 = Polydispersity index (PDI)		Minimize	0.075	0.077 ± 0.005	+ 2.6
Y_3 = Entrapment efficiency (%)		Maximize	74.99	71.58 ± 1.22	-4.7
Statistical summary					
	F-value	**P-value***	**R^2**	**Lack of Fit**	**Comments**
Nanoparticle size	6.02	0.0137	0.8856	0.0524	Significant
Polydispersity index	3.62	0.0426	0.4550	0.0512	Significant
Entrapment efficiency	5.69	0.016	0.8797	0.1205	Significant
* Data with a p-value of < 0.05 were considered statistically significant.					
** Mean of three replicates ± SD					

Table 3. Observed levels, constraints and prediction errors of dependent variables in Box-Behnken design.

Table 3 *is attached*

3.1.1. Influence of variables on nanoparticle size

Nanoparticle size was assessed due to its effect on physicochemical properties such as stability, degradability, drug delivery and release. Generally, the particle size of PHBV-ACZ NPs was in the range of 250.9 ± 7.4 nm (trial no. 3) to 364.8 ± 0.93 nm (trial no. 15) by varying the limits of individual parameters. The polynomial equation for nanoparticle size generated after the data modelling can be described by the following equation:

$$Y_1 = 294.92 - 18.86X_1 - 21.50X_2 - 20.41X_3 - 23.35X_1X_2 - 3.63X_1X_3 + 23.25X_2X_3 + 23.78X_1^2 + 11.35X_2^2 - 12.07X_3^2$$

Y_1 refers to nanoparticle size, X_1, X_2, and X_3 shows the concentration of PHBV, PVA, and ACZ, respectively. The independent parameters present the most suitable for the second-order polynomial model with F-value 6.02 (p = 0.013) and non-significant lack of fit (p = 0.0524). A high r^2 value (0.885) indicates a sensible relationship between experimental and predicted values (Table 3). According to the response surface analysis plot, increase in PHBV concentration at low PVA levels indicated an initial downward trend at low to moderate levels, followed by an ascending pattern at moderate to high levels. However, at high PVA level, the increase in PHBV concentration exhibited a slight downward trend in nanoparticle size. On the contrary, at high PHBV level, increase in PVA concentration showed a mild declining trend on the nanoparticle size. Based on the results from ANOVA, the PHBV concentration (p values = 0.021) and the interaction of PHBV and PVA concentrations (p values = 0.036) had significant effects on the size of the nanoparticles while the other variables had no significant effect on the nanoparticle size (p > 0.05) (Fig. 1A). As shown in Fig. 1A, at constant ACZ concentration, PHBV and PVA concentration positively affect the particle size of PHBV-ACZ NPs due to their direct effects on viscosity.

3.1.2. Influence of variables on polydispersity index

PDI, a measure of sample heterogeneity, was acquired in the range of 0.036 ± 0.038 (trial no. 14) to 0.254 ± 0.013 (trial no. 7) using specified level combinations of different independent variables. The following linear equation describes the relationship between PDI (Y_2) and independent variables:

$$Y_2 = 0.0955 - 0.0009X_1 - 0.0456X_2 - 0.0265X_3$$

As the independent parameters fit well with the linear model with an F-value of 3.62 (p = 0.0426) and non-significant lack of fit (p = 0.0512), the given model can be used to predict the PDI of PHBV-ACZ NPs. The ANOVA results indicated that the PVA concentration (p = 0.013) was the most main factor affecting PDI (Fig. 1B). As shown in Fig. 1B, at overall PHBV levels, the decrease in PVA concentration exhibited a slight downward trend in nanoparticle size.

3.1.3. Influence of variables on entrapment efficiency

The EE% of optimized formulation was determined in the range 41.18 ± 3.86% (trial no. 16) to 71.71 ± 2.98% (trial no. 6). According to the data obtained from the combination of different independent factors, the polynomial model was determined as the most appropriate model for %EE. The effect of independent factors on %EE (Y_3) can be explained by the following mathematical polynomial equation:

$$Y_3 = 46.41 + 2.66X_2 - 7.39X_3 - 6.11X_2X_3 + 13.27X_3^2 - 7.14X_2X_3^2$$

The quadratic model of the formulation has a significant F-value of 23.71 (p < 0.0001) and a non-significant lack of fit 0.942 (p = 0.558). The R^2 value (0.915) demonstrates a good adequacy and fit between experimental and predicted values. According to the ANOVA results, ACZ concentration was the most important factor-affecting %EE (p < 0.0001), whereas PHBV and PVA concentration had no significant effects (p > 0.05). As shown in Fig. 1C, decreasing ACZ concentration resulted in an increase in EE level. This behavior of EE can be attributed to the strength of the binding forces between PHBV and drug. Since ACZ is a weak acid, an electrostatic repulsion occurs between the drug anion and the negatively charged polymers. This repulsion offers lower loading capacity compared to positively charged polymers [53].

Figure 1 is attached

3.1.4. Optimized formulation and model validation study

Numerical optimization of the independent variables was determined by minimizing particle size and size distribution and maximizing %EE. Optimized levels for PHBV, PVA, and ACZ concentration were identified as 1.75%, 1.5%, and 0.1% w/v, respectively. The predicted nanoparticle size, PDI value, and drug entrapment efficiency were also estimated as 254.46 nm, 0.075, and 74.99%, respectively (Table 3). To verify the prediction, PHBV-ACZ NP were synthesized using optimum values and physicochemical properties of optimized nanoparticles offer a particle size of 253.20 ± 0.55 nm, PDI of 0.077 ± 0.005, and EE of 71.58 ± 1.22%, which were quite closer to the predicted values (Table 3). The validity of the BBD for optimized nanoparticle synthesis was confirmed with prediction errors of less than 5% (Table 3) [54]. The production efficiency of nanoparticles was calculated according to the formula below and it was determined that the particles were obtained with a 91% yield.

% Yield: Total nanoparticle weight / Starting polymer amount × 100

3.2. Size distributions, zeta potentials, dimensions of nanoparticles

Dynamic light scattering technique (DIS) was used to measure the size, PDI, and zeta potential of NPs. The average size, PDI, and zeta potential of optimized PHBV-ACZ NPs obtained after aqueous dispersion was measured as 253.20 ± 0.55 nm, 0.077 ± 0.005, and − 18.7 ± 0.627 mV, respectively. Monodisperse size distribution of NPs can be inferred from Fig. 2. SEM images reveal a very close agreement between the NP size in the non-aqueous phase and the NP size acquired by the DLS method. SEM images of PHBV-ACZ NP (Fig. 2B-D) and empty PHBVs (Fig. 2E-G) show that the nanoparticles are in monodisperse and spherical form. In the PHBV-ACZ NP surface morphology, they exhibit a smooth surface without any clumping. PHBV nanoparticles showed a negative surface charge in the range of -12.6 and − 30.7 mV (Table 1). The data obtained are compatible with the data in the literature [55].

Figure 2 is attached

3.3. ACZ release profiles

The amount of drug administered per encapsulated amount was determined as 15.4%. The release profile of the optimized formulation of ACZ loaded nanoparticles is presented in Fig. 3. Since ACZ gives a peak at 293 nm wavelengths in PBS (pH = 7.4) solution medium, a standard calibration graph was prepared according to this wavelength in the drug release study. In the release profile from the PHBV-ACZ NP, it was observed that it continued in a controlled manner after the first burst release, and and 32% of

the drug was released after 6 days. ACZ exhibited a slow-release profile from PHBV nanoparticles in the stationary phase, with a relatively rapid release of 15.65% of the drug in the first 24 hours.

Figure 3 is attached

In 1950, Miller et al. discovered the synthesis of acetazolamide, methazolamide, and ethoxzolamide, the first-generation Carbonic Anhydrase inhibitors [56]. Acetazolamide and methazolamide were used as active molecules in many different indications, especially in glaucoma [41, 57]. ACZ has been used widely for many years in the treatment of glaucoma all over the world. In the literature, ACZ has been preferred in many studies evaluating the ocular efficacy and toxicity of Carbonic anhydrase inhibitors (CAI) [41, 58]. Since ACZ has been widely used in clinical applications and eye diseases for many years, there is no doubt about its safety. Also, there are case reports and case series about the use of ACZ in DRP [59, 60].

3.4. Stability/degradation time of nanoparticles

One of the important factors affecting the drug release profile is the degradation rate of nanoparticles [47]. Degradation studies were carried out at two different temperatures, 37°C (Fig. 3B) and 4°C (Fig. 3C), and each measurement was repeated 3 times. As can be seen in Fig. 3B-C, increasing the temperature caused the degradation rate of the nanoparticles to increase.

Thermal degradation of PHBV occurs by a random β-elimination reaction involving a six-membered ring transition state. On the one hand, carbon atoms in the α-position have a strong electron-donating effect against ester oxygen. On the other hand, the periphery group of the methylene group in the β-position has a negative inductive effect on the ester oxygen. During the initial stages of the thermal depolymerization of PHBV, the crotonate end group PHBV and the low molecular weight PHBV are produced by the chain cutting process. As a result of this process, crotonic acid and various oligomers can be transformed into more structures in the form of propylene, CO_2, acetaldehyde, and flax [3].

3.5. *In vitro* evaluation of the efficiency and safety of the synthesized nanoparticular drug delivery system

3.5.1. Cytotoxicity of PHBV-ACZ NPs on HRMEC and human monocyte/macrophage cell line (THP-1)

In the study; PHBV NP, PHBV-ACZ NP., ACZ loaded and steroid coated PHBV nanoparticle (PHBV-ACZ-St NP), steroid, and ACZ (1, 10, 50, 100, and 250 µg/ml) toxicity on HRMEC by WST-1 test determined. The WST-1 test is a test used to determine cell viability. Whether the materials developed are cytotoxic or not or their cytotoxicity rates can be determined with this test. In the WST-1 test, the wells in the first column of the plate were used as control and each nanoparticle at different concentrations was studied in 6 replicates. The average of the absorbance taken from the control wells was accepted as 100% and compared with the average absorbance taken from the test wells and the toxicity of the nanoparticles was determined (Fig. 4). When the cytotoxicity of the groups exposed to PHBV NP and PHBV-ACZ-St NP were compared, there was no significant difference ($P > 0.05$), and both groups were not cytotoxic to HRMEC cells. When the cytotoxicity of PHBV-ACZ NP, PHBV-ACZ-St NP and steroid exposed groups were examined, it was observed that PHBV-ACZ NP and PHBV-ACZ-St NP were not cytotoxic on HRMEC cells ($P < 0.05$). According to the cytotoxicity results of the groups treated with free ACZ and PHBV-ACZ NP, it was determined that free ACZ was cytotoxic to cells at a concentration above 50 µg/ml ($P < 0.05$, however, when encapsulated with PHBV, it was not cytotoxic to cells ($P > 0.05$). Accordingly, 94% of HRMEC interacting with PHBV-ACZ-St NP at a concentration of 250µg/ml are alive or the nanoparticle is 6% cytotoxic. When the results are compared, as the concentration increases, the cytotoxicity of the nanoparticles on the cells also increases. At a concentration of 250µg/ml, the cells show 90% viability. This shows us that the cytotoxicity of the particles on cells is very low and is suitable for *in vivo* applications (Fig. 4A).

When the results obtained from THP-1 cells are compared, as the concentration increases, the cytotoxicity of the nanoparticles on the cells also increases. At a concentration of 250µg/ml, the cells show 90% viability. There appears to be no statistically significant difference between the cytotoxicity of the particles on THP-1 cells ($P > 0.05$). An increase in the number of THP-1 cells is observed due to the increase in the steroid and ACZ concentration ($P < 0.05$). Steroid and ACZ have an inflammatory effect on cells [61], so THP-1 cells create response by increasing. In this way, tissue damage is tried to be prevented (Fig. 4B). In the study of Lemarchand et al. in 2006; investigated the ability of coating structures with Dexamethazone to alter interactions with the biological

environment. The effect of Dexamethasone coating on the phagocytosis and toxicity of nanoparticles was investigated by human TPH-1 and J774 murine macrophage-like cell lines. It was determined that the modification of the surface with DEX significantly reduced cytotoxicity and increased proliferation in THP-1 and J774 cell lines [62].

Borhani H. et al. determined the toxic dose of carbonic anhydrase inhibitor (CAI) as 1mg in rabbits [58]. The free form of ACZ, which is a CAI, has a toxic effect on cells. As the cells that interacted with ACZ at 250µg/ml concentration show 73.977% viability, cells that interacted with PHBV-ACZ NPs at the same concentration show 90.631% viability. The use of nanoparticular systems has been one of the most used methods in recent years to reduce cytotoxicity in the use of active substances with toxic effects. Nanoparticles structures, both provide a controlled release by extending the release time of the loaded substances, and ensure that the active substance remains in the effective dose range in the environment. Also, they provide a more functional application opportunity by reducing the cytotoxicity of the active ingredients. PHBV is a biocompatible polymer. The use of structures obtained from biocompatible polymers provides advantages in terms of their non-toxicity and degradation products. Cells that interacted with PHVB NP at a concentration of 250µg/ml show 96.626% viability.

Figure 4 is attached

3.5.2. The effect of nanoparticles on cytokine response using THP-1 cell line

TNF-alpha and IL-10 release in PMA-stimulated THP-1 cells was approximately 0.209pg/ml and 0.250pg/ml, respectively. Standard cell culture medium was used as negative control in the study. Other groups were evaluated by comparison with the negative control. When the results were examined, it was determined that free ACZ and steroid together with other groups did not stimulate TNF alpha expression of macrophages ($P > 0.05$). When the TNF alpha values between the groups were compared, no significant difference was observed between them ($P > 0.05$) (Fig. 5A). It was observed that free steroid stimulated IL10 expression of THP-1 cells at 250ug/ml concentration ($P < 0.05$), but not TNF alpha level ($P > 0.05$). Other groups did not induce IL10 expression of cells ($P > 0.05$) (Fig. 5B).

Figure 5 is attached

Steroids such as dexamethasone inhibit the expression of inflammatory mediators. Therefore, they both increase the inflammation of cells and are used in the treatment of many immune-mediated inflammatory diseases. Abraham et al. investigated the role of DUSP1 in the anti-inflammatory effect of dexamethasone (Dex) [63]. In this context; The effects of DUSP1 gene activity on the anti-inflammatory function of dexamethasone were tested using the in vivo skin air sac model and IL-1 and TNF alpha levels were determined. In the study, it was determined that the use of dexamethasone suppressed the expression of IL-1 and TNF alpha.

3.5.3. Hemocompatibility of nanoparticles

If the percentage of hemolysis caused by the materials used is less than 5%, it is accepted as hemocompatible in the literature [64]. Nanoparticles in different formulations prepared within the scope of the study are hemocompatible at low concentrations. More than 5% hemolysis is seen at and above 100µg/ml concentration. However, the highest hemolysis value (11.155%) was obtained from serum interacting with PHBV-ACZ-St NP at the concentration of 250µg/ml. When the hemolysis results are evaluated together with the cytotoxicity results obtained at the same concentration, the hemolysis value is a tolerable value for *in vivo* experiments (Fig. 6A) ($n = 3$).

3.5.4. Creation of DRP model in Human Retinal Microvascular Endothelial Cell Culture

The formation of the DRP pattern in the HRMEC was determined by TEER measurement. In single-layer cells (monolayer), there is a gradual increase in TEER measurement as the intercellular spaces are closed. In the literature, TEER value for HRMEC planted in 12 well inserts has been reported as 20–40 ohm/cm^2 (Suarez et al. 2014). Since the barrier function is impaired in the DRP cell culture model, the resistance values obtained as a result of TEER measurements decrease compared to normal values [51]. There was a time-dependent decrease in TEER measurements of cells treated with a VEGF-containing medium. In the study, VEGF at a concentration of 150ng/ml was used for *in vitro* DRP formation.

3.5.5. TEER Measurement

TEER values of 3 different NP formulations (PHBV NP, PHBV-ACZ NP, PHBV-ACZ-St NP), ACZ, and steroid were determined in the study.

Although TEER values obtained from cells in control group inserts showed a certain decrease, they remained stable. The decrease in the 48 hour is since the cells cannot find a surface to be attached to and ruptures from the surface after a certain time since the cells cover the entire insert surface. A decrease in the TEER value of cells incubated with VEGF-containing medium and empty PHBV-NP occurs over time. In the DRP cell culture model, it is expected that VEGF in the environment damages the cell surface and PHBV does not have a therapeutic effect (Fig. 6B).

While the TEER value of cells exposed to PHBV-ACZ NP and PHBV-ACZ-St NP initially decreased due to the presence of VEGF, a significant increase in TEER value was observed with the addition of nanoparticles to the medium ($P < 0.05$). With the release of ACZ loaded on nanoparticles into the environment, the effect of VEGF decreases, and treatment is applied at the cellular level *in vitro*. The increase in TEER value was higher in the PHBV-ACZ-St NP group. First, the release of steroid into the environment initiated the treatment process, and ACZ released from the particles both increased and continued this treatment (Fig. 6B) (n = 3).

Figure 6 is attached

3.5.6. Permeability Analysis

Cell permeability tests performed in the HRMEC are used in the *in vitro* evaluation of DRP. The differences between the groups were compared by measuring the permeability values of the control, VEGF, VEGF-nanoparticle groups (PHBV NP, PHBV-ACZ NP, PHBV-ACZ-St NP) ACZ, and steroid. In the permeability analysis, a blank insert (without HRMEC) was used as a control. The average of the concentrations taken from the control was accepted as 100% and the permeability percentages of the cells in the other inserts were determined accordingly (Table 4). Each experiment was repeated 3 times and averaged.

Table 4
Permeability percentages of HRMEC cells incubated in medium with and without VEGF

	Permeabilite %	Std. Dev.
Medium	**100,0**	**2,0**
HRMEC	**57,4**	**14,0**
HRMEC/VEGF	**88,5**	**18,0**
HRMEC/VEGF/PHBV	**86,2**	**5,8**
HRMEC/VEGF/PHBV-ACZ NP	**86,8**	**22,6**
HRMEC/VEGF/PHBV-ACZ-St NP	**43,8**	**5,3**
HRMEC/VEGF/ACZ	**76,1**	**13,9**
HRMEC/VEGF/Steroid	**57,6**	**15,9**

Percentages of permeability of cells incubated with the medium are quite low compared to other groups. This indicates that the fluorescent material passage to the lower compartment is low due to the cells covering the insert surface. The percentage of permeability of cells incubated with VEGF-containing medium is the highest compared to other groups. In the DRP model, it is an expected situation as a result of damage to the cell surface of VEGF in the environment (Table 4). Percentages of permeability of the cells exposed to PHBV NP and PHBV-ACZ NP were determined at a value close to the permeability percentage of the cells incubated with media containing VEGF. It is due to the lack of effect of PHBV NP and ACZ on the proliferation and repair of cells. It is seen that cells exposed to PHBV-ACZ-St NP allow a decrease in permeability and less fluorescent substance passage from HRMEC cells. First, the release of the steroid into the environment initiated the cellular therapy process and the ACZ released from the nanoparticles both increased and continued this treatment (Table 4).

Table 4. Permeability percentages of HRMEC cells incubated in medium with and without VEGF

Table 4 *is attached*

3.5.7. Cell Based ELISA

The amount of intercellular connection structures such as Claudin-5, Caveolin, VE-Cadherin and carrier proteins such as ZO-1, PLVAP, laminin on the cell surface and their changes after exposure to active substances were determined using commercial kits. Proteins such as Claudin-5, Caveolin and VE-Cadherin have been shown to be necessary for the regulation of permeability in barrier structures such as the blood brain barrier and blood retina barrier [65–67].

VEGF is a strong angiogenesis and vascular permeability factor [68]. In diabetes, increased retinal VEGF levels correspond to Blood-retinal barrier (BRB) degradation in humans [69]. The presence of VEGF in the environment causes a decrease in the levels of the junction protein VE-Cad and junction-related protein ZO-1, as well as the tight junction proteins claudin-5, which are found on the cell surface ($P < 0.05$) [70]. Literature show that the presence of VEGF initially reduces the levels of proteins on the cell surface by damaging them, but these levels increase after 24 hours. A significant increase in VE-Cad expression was observed 48 hours after VEGF addition (Fig. 7). When the Claudin-5 expression of HRMEC cells is examined; it was observed that PHBV-ACZ NP increased Claudin-5 expression, but this increase was not statistically significant ($P > 0.05$). However, PHBV-ACZ-St NP significantly increased the expression of Claudin-5 in HRMEC cells ($P < 0.05$). ACZ and steroid administration alone did not significantly increase Claudin expression in HRMEC cells ($P > 0.05$).

In cells incubated with media containing VEGF occurred increased expression of cell surface proteins. There is an increase in the intercellular protein concentration in cells exposed to PHBV-ACZ NP. The intercellular protein concentration in the well to which PHBV-ACZ-St NP were added increased an average of 2.5 times (Fig. 7). Both the controlled release of ACZ and the presence of the steroid in the environment provided *in vitro* treatment as well as stimulated the cells. It was observed that PLVAP level increased in HRMEC cells interacted with VEGF ($P < 0.05$). However, ACZ and ACZ loaded nanoparticles alone did not induce PLVAP expression ($P > 0.05$). When steroids were added to the cells together with ACZ loaded nanoparticles, it was observed that there was a significant increase in the expression of PLVAP in the cells ($P < 0.05$) and it was understood that this increase was not due to the steroid alone ($P > 0.05$). The interaction of VEGF with HRMEC cells significantly induced CAV-1 release ($P < 0.05$). When VEGF-treated HRMEC cells were interacted with PHBV nanoparticles alone, no significant change in CAV-1 expression was observed ($P < 0.05$). However, ACZ loaded PHBV nanoparticles and ACZ alone were found to stimulate CAV-1 expression of HRMEC cells ($P < 0.05$).

In vitro studies in the literature have indicated that the destruction of the blood retinal barrier due to VEGF triggers phosphorylation and ubiquitination, leading to the rearrangement of tight junctions [71, 72]. In the study of David A. Antonetti et al. (1999), the mechanism by which VEGF regulates paracellular permeability in rats was investigated. Intraocular injection of VEGF caused a posttranslational modification of occludin and tyrosine phosphorylation of ZO-1. It has been determined that phosphorylation of occludin and ZO-1 likely causes an increase in regulated endothelial permeability. Again, in a previous study they conducted in 1998, it was shown that chronic incubation of bovine retinal endothelial cells (BREC) with VEGF reduced the content of occludin after 3–6 hours and caused by changes in barrier permeability properties [73].

Using the cell-based ELISA, a transient decrease in the expression of PLVAP, the plasmalemma vesicle-associated protein, was observed in HRME cells stimulated with VEGF. It was determined that the expression of PLVAP levels in cells incubated with VEGF at the end of 24 hours was low. After 48 hours in cells incubated with VEGF, an increase in intercellular proteins is observed (Fig. 7) [74, 75]. In the study conducted by Klassen et al., it was determined that the expression of endothelial cell tight junction genes and especially occludin and claudin-5 decreased after exposure to VEGF in diabetic retina and BRECs. Expression of 6 of the 11-vesicular transport-related genes was upregulated by induction of diabetes. PLVAP transcription was significantly induced by VEGF in the diabetic retina and BRECs. In the VEGF-stimulated diabetic retina, Ocludin and klaudin-5 showed a transient down-regulation, while induction of caveolin-1 and PLVAP expression was observed. Expression of laminin showed stable expression in groups incubated with VEGF throughout the entire experiment. Since VEGF does not damage the laminin on the cell surface, no change is observed in its expression ($P < 0.05$). However, a significant increase in the amount of laminin was seen in the groups incubated with VEGF and with steroid-containing nanoparticles and steroids. Since the steroid stimulates cell proliferation, it has been determined that it causes an increase in both total protein amount and laminin expression (Fig. 7).

Figure 7 is attached

4. Conclusion

VEGF plays a key role in the development of DRP. Based on this information, anti-VEGF agents and steroids that act to suppress the VEGF effect are used in its treatment. In the study, nanoparticles (NP) loaded with CAI were synthesized to be used in DRP treatment, and the efficacy and safety of these nanoparticles were investigated by *in vitro* studies. The toxicity and hemocompatibility of nanoparticles of different formulations and concentrations were investigated. Toxicity tests were performed with HRMEC and THP-1 cells, and cells showed 90% viability in both cell lines exposed to nanoparticles at a concentration of 250µg/ml. When the hemolysis results are evaluated together with the cytotoxicity results obtained at these concentrations, the hemolysis values are in the tolerable range *in vivo* experiments. HRMEC was exposed to VEGF to create an *in vitro* DRP model and characterized by TEER. Also, to investigate the damage caused by VEGF in the blood-retina barrier and the change caused by the addition of nanoparticles, the regulation in permeability and intercellular junction proteins were examined. While the TEER value of the cells initially decreased due to the presence of VEGF, a significant increase was observed in the TEER value with the addition of ACZ loaded nanoparticles to the medium. Consequently, the permeability also decreased.

Declarations

ETHICAL STATEMENT

Ethics approval and consent to participate:

No human or animal participants were used in the study.

Availability of data and materials

The datasets generated during and analyzed during the current study are available from the corresponding author (Nagihan UGURLU) and Ebru ERDAL on reasonable request.

Competing interests

Financial interests: Authors Ebru ERDAL and Soheil Malekghasemi declare that they have no financial interests.

Nagihan UGURLU and Murat DEMIRBILEK have received research funding from The Scientific And Technological Research Council Of Turkey (TUBITAK).

Funding/ Acknowledgements

The studies were financially supported by TUBITAK with the project number 216S700.

Authors' contributions

All authors contributed to the study conception and design. Material preparation, data collection and analysis were performed by Soheil Malekghasemi. *In vitro* experiment of nanoparticles (cytotoxicity, cytokine response, hemocompatibility, TEER and permeability tests) were performed by Ebru ERDAL. Creation of DRP model in vitro, data collection and analysis were performed by Nagihan UGURLU and Murat DEMIRBILEK. The first draft of the manuscript was written by Nagihan UGURLU and all authors commented on previous versions of the manuscript. All authors read and approved the final manuscript.”

References

1. **Yau J, Rogers SL, Kawasaki R., Lamoureux EL, Kowalski JW, Bek T, Chen S, Dekker J, Fletcher A, Grauslund J (2012) Meta-analysis for eye disease (metaeye) study group. Global prevalence and major risk factors of diabetic retinopathy. Diabetes care 35:556–564. https://doi.org/10.2337/dc11-1909**

2. Tan GS, Cheung N, Simó R, Cheung GC, Wong TY (2017) Diabetic macular oedema. The lancet Diabetes & endocrinology 5:143 – 55. https://doi.org/10.1016/S2213-8587(16)30052-3
3. Nguyen S, Yu G, Marchessault RH (2002) Thermal degradation of poly (3-hydroxyalkanoates): Preparation of well-defined oligomers. Biomacromolecules 3:219–24. https://doi.org/10.1021/bm0156274
4. Virgili G, Parravano M, Evans JR, Gordon I, Lucenteforte E (2018) Anti-vascular endothelial growth factor for diabetic macular oedema: A network meta-analysis. Cochrane Database of Systematic Reviews 10. https://doi.org/10.1002/14651858.CD007419.pub5
5. Shikari H, Silva PS, Sun JK (2014) Complications of intravitreal injections in patients with diabetes. Presented at Seminars in ophthalmology, Taylor & Francis. 29:276–289. https://doi.org/10.3109/08820538.2014.962167
6. Browning DJ, Stewart MW, Lee C (2018) Diabetic macular edema: Evidence-based management. Indian journal of ophthalmology 66:1736. https://doi.org/10.4103/ijo.IJO_1240_18
7. Wecker T, Ehlken C, Bühler A, Lange C, Agostini H, Böhringer D, Stahl A (2017) Five-year visual acuity outcomes and injection patterns in patients with pro-re-nata treatments for amd, dme, rvo and myopic cnv. British Journal of Ophthalmology 101:353–359. https://doi.org/10.1136/bjophthalmol-2016-308668
8. Dugel PU, Layton A, Varma R (2016) Diabetic macular edema diagnosis and treatment in the real world: An analysis of medicare claims data (2008 to 2010). Ophthalmic Surgery, Lasers and Imaging Retina, 47:258–267. https://doi.org/10.3928/23258160-20160229-09
9. Kiss S, Liu Y, Brown J, Holekamp NM, Almony A, Campbell J, Kowalski JW (2014) Clinical utilization of anti-vascular endothelial growth-factor agents and patient monitoring in retinal vein occlusion and diabetic macular edema. Clinical ophthalmology (Auckland, NZ) 8:1611. https://doi.org/10.2147/OPTH.S60893
10. Del Amo EM, Urtti A (2008) Current and future ophthalmic drug delivery systems: A shift to the posterior segment. Drug discovery today 13:135–143. https://doi.org/10.1016/j.drudis.2007.11.002
11. Short BG (2008) Safety evaluation of ocular drug delivery formulations: Techniques and practical considerations. Toxicologic pathology 36:49–62. https://doi.org/10.1177/0192623307310955
12. Shah SU, Maturi RK (2017) Therapeutic options in refractory diabetic macular oedema. Drugs 77:481–92. https://doi.org/10.1007/s40265-017-0704-6
13. Kompella UB, Amrite AC, Ravi RP, Durazo SA (2013) Nanomedicines for back of the eye drug delivery, gene delivery, and imaging. Progress in retinal and eye research 36:172–198. https://doi.org/10.1016/j.preteyeres.2013.04.001
14. Geroski DH, Edelhauser HF (2000) Drug delivery for posterior segment eye disease. Investigative Ophthalmology & Visual Science 41:961–964.
15. Kaur IP, Kakkar S (2014) Nanotherapy for posterior eye diseases. Journal of Controlled Release 193:100–112. https://doi.org/10.1016/j.jconrel.2014.05.031
16. Diebold Y, Calonge M (2010) Applications of nanoparticles in ophthalmology. Progress in retinal and eye research 29:596–609. https://doi.org/10.1016/j.preteyeres.2010.08.002
17. Reimondez-Troitiño S, Csaba N, Alonso M, De La Fuente M (2015) Nanotherapies for the treatment of ocular diseases. European Journal of Pharmaceutics and Biopharmaceutics 95:279–293. https://doi.org/10.1016/j.ejpb.2015.02.019
18. Koller M (2018) Biodegradable and biocompatible polyhydroxy-alkanoates (pha): Auspicious microbial macromolecules for pharmaceutical and therapeutic applications. Molecules 23:362. https://doi.org/10.3390/molecules23020362
19. Masood F, Yasin T, Hameed A (2015) Polyhydroxyalkanoates–what are the uses? Current challenges and perspectives. Critical reviews in biotechnology 35:514–521. https://doi.org/10.3109/07388551.2014.913548
20. Brigham CJ, Sinskey AJ (2012) Applications of polyhydroxyalkanoates in the medical industry. International Journal of Biotechnology for Wellness Industries 1:53–60. https://doi.org/10.6000/1927-3037.2012.01.01.03
21. Volova T, Shishatskaya E, Sevastianov V, Efremov S, Mogilnaya O (2003) Results of biomedical investigations of phb and phb/phv fibers. Biochemical engineering journal 16:125–133. https://doi.org/10.1016/S1369-703X(03)00038-X
22. Showalter MR, Cajka T, Fiehn O (2017) Epimetabolites: Discovering metabolism beyond building and burning. Current opinion in chemical biology 36:70–76. https://doi.org/10.1016/j.cbpa.2017.01.012

23. Zinn M, Witholt B, Egli T (2001) Occurrence, synthesis and medical application of bacterial polyhydroxyalkanoate. Advanced drug delivery reviews 53:5–21. https://doi.org/10.1016/s0169-409x(01)00218-6
24. Yu X, Zhang Z, Yu J, Chen H, Li X (2018) Self-assembly of a ibuprofen-peptide conjugate to suppress ocular inflammation. Nanomedicine: Nanotechnology, Biology and Medicine 14:185–193. https://doi.org/10.1016/j.nano.2017.09.010.
25. Aksungur P, Demirbilek M, Denkbaş EB, Vandervoort J, Ludwig A, Ünlü N (2011) Development and characterization of cyclosporine a loaded nanoparticles for ocular drug delivery: Cellular toxicity, uptake, and kinetic studies. Journal of Controlled Release 151:286–94. https://doi.org/10.1016/j.jconrel.2011.01.010
26. Achouri D, Alhanout K, Piccerelle P, Andrieu V (2013) Recent advances in ocular drug delivery. Drug development and industrial pharmacy 39:1599–1617. https://doi.org/10.3109/03639045.2012.736515
27. Almeida H, Amaral MH, Lobão P, Silva AC, Loboa JMS (2014) Applications of polymeric and lipid nanoparticles in ophthalmic pharmaceutical formulations: Present and future considerations. Journal of Pharmacy & Pharmaceutical Sciences 17:278–293. https://doi.org/10.18433/j3dp43
28. Lakhani P, Patil A, Majumdar S (2018) Recent advances in topical nano drug-delivery systems for the anterior ocular segment. Therapeutic delivery 9:137–153. https://doi.org/10.4155/tde-2017-0088
29. Gonzalez VH, Campbell J, Holekamp NM, Kiss S, Loewenstein A, Augustin AJ, Ma J, Ho AC, Patel V, Whitcup SM (2016) Early and long-term responses to anti–vascular endothelial growth factor therapy in diabetic macular edema: Analysis of protocol i data. American journal of ophthalmology 172:72–79. https://doi.org/10.1016/j.ajo.2016.09.012
30. Bressler NM, Beaulieu WT, Maguire MG, Glassman AR, Blinder KJ, Bressler SB, Gonzalez VH, Jampol LM, Melia M, Sun JK (2018) Early response to anti–vascular endothelial growth factor and two-year outcomes among eyes with diabetic macular edema in protocol t. American journal of ophthalmology 195:93–100. https://doi.org/10.1016/j.ajo.2018.07.030
31. Santos AR, Costa MÂ, Schwartz C, Alves D, Figueira J, Silva R, Cunha-Vaz JG (2018) Optical coherence tomography baseline predictors for initial best-corrected visual acuity response to intravitreal anti-vascular endothelial growth factor treatment in eyes with diabetic macular edema: The chartres study. Retina 38:1110–1119. https://doi.org/10.1097/IAE.0000000000001687
32. Brown DM, Nguyen QD, Marcus DM, Boyer DS, Patel S, Feiner L, Schlottmann PG, Rundle AC, Zhang J, Rubio RG (2013) Long-term outcomes of ranibizumab therapy for diabetic macular edema: The 36-month results from two phase iii trials: Rise and ride. Ophthalmology 120. https://doi.org/10.1016/j.ophtha.2013.02.034
33. Elman MJ, Aiello LP, Beck RW, Bressler NM, Bressler SB, Edwards AR, Ferris FL, Friedman SM, Glassman AR, Miller KM, Scott IU, Stockdale CR, Sun JK (2010) Randomized trial evaluating ranibizumab plus prompt or deferred laser or triamcinolone plus prompt laser for diabetic macular edema. Ophthalmology, 117:1064–1077. https://doi.org/10.1016/j.ophtha.2010.02.031
34. Bressler SB, Qin H, Beck RW, Chalam KV, Kim JE, Melia M, Wells JA (2012) Diabetic Retinopathy Clinical Research Network. Factors associated with changes in visual acuity and central subfield thickness at 1 year after treatment for diabetic macular edema with ranibizumab. Archives of Ophthalmology 130:1153–1161. https://doi.org/10.1001/archophthalmol.2012.1107
35. Sun JK, Lin MM, Lammer J, Prager S, Sarangi R, Silva PS, Aiello LP (2014) Disorganization of the retinal inner layers as a predictor of visual acuity in eyes with center-involved diabetic macular edema. JAMA ophthalmology 132:1309–1316. https://doi.org/10.1001/jamaophthalmol.2014.2350
36. Sun JK, Radwan SH, Soliman AZ, Lammer J, Lin MM, Prager SG, Silva PS, Aiello LB, Aiello LP (2015) Neural retinal disorganization as a robust marker of visual acuity in current and resolved diabetic macular edema. Diabetes 64:2560–2570. https://doi.org/10.2337/db14-0782
37. Kita T, Clermont AC, Murugesan N, Zhou Q, Fujisawa K, Ishibashi T, Aiello LP, Feener EP (2015) Plasma kallikrein-kinin system as a vegf-independent mediator of diabetic macular edema. Diabetes 64:3588–3599. https://doi.org/10.2337/db15-0317.
38. Clermont A, Chilcote TJ, Kita T, Liu J, Riva P, Sinha S, Feener EP (2011) Plasma kallikrein mediates retinal vascular dysfunction and induces retinal thickening in diabetic rats. Diabetes 60:1590–1598. https://doi.org/10.2337/db10-1260.
39. Urias EA, Urias GA, Monickaraj F, McGuire P, Das A (2017) Novel therapeutic targets in diabetic macular edema: Beyond vegf. Vision research 139:221–227. https://doi.org/10.1016/j.visres.2017.06.015
40. Hussain RM, Ciulla TA (2016) Treatment strategies for refractory diabetic macular edema: Switching anti-vegf treatments, adopting corticosteroid-based treatments, and combination therapy. Expert opinion on biological therapy 16:365–374. https://doi.org/10.1517/14712598.2016.1131265

41. Kaur IP, R. Smitha, D. Aggarwal, M. Kapil, Acetazolamide: Future perspective in topical glaucoma therapeutics, International Journal of Pharmaceutics, 248 (2002) 1–14. https://doi.org/10.1016/s0378-5173(02)00438-6
42. Gaballa SA, Kompella UB, Elgarhy O, Alqahtani AM, Pierscionek B, Alany RG, Abdelkader H (2021) Corticosteroids in ophthalmology: Drug delivery innovations, pharmacology, clinical applications, and future perspectives. Drug Delivery and Translational Research 11:866–893. https://doi.org/10.1007/s13346-020-00843-z
43. Sahana B, Santra K, Basu S, Mukherjee B (2010) Development of biodegradable polymer based tamoxifen citrate loaded nanoparticles and effect of some manufacturing process parameters on them: A physicochemical and in-vitro evaluation. International journal of nanomedicine 5:621. https://doi.org/10.2147/IJN.S9962.
44. Rizkalla N, Hildgen P (2005) Artificial neural networks: Comparison of two programs for modeling a process of nanoparticle preparation. Drug development and industrial pharmacy 31:1019–1033. https://doi.org/10.1080/03639040500306294.
45. Kumar A, Ahuja M (2013) Carboxymethyl gum kondagogu–chitosan polyelectrolyte complex nanoparticles: Preparation and characterization. International journal of biological macromolecules 62:80–84. https://doi.org/10.1016/j.ijbiomac.2013.08.035
46. Gannu R, Yamsani VV, Yamsani SK, Palem CR, Yamsani MR (2009) Optimization of hydrogels for transdermal delivery of lisinopril by box–behnken statistical design. Aaps Pharmscitech 10:505–14. https://doi.org/10.1208/s12249-009-9230-5
47. Souto E, Müller R (2006) The use of sln® and nlc® as topical particulate carriers for imidazole antifungal agents. Die Pharmazie-An International Journal of Pharmaceutical Sciences 61:431–437. PMID: 16724541.
48. Mahajna S, Azab M, Zaid H, Farich BA, Al Battah F, Mashner S, Saad B (2015) In vitro evaluations of cytotoxicity and anti-inflammatory effects of peganum harmala seed extracts in thp-1-derived macrophages. European Journal of Medicinal Plants 165–175. https://doi.org/10.9734/EJMP/2015/13267
49. Mocan T (2013) Hemolysis as expression of nanoparticles-induced cytotoxicity in red blood cells. BMBN,1:7–12,
50. Suarez S, McCollum GW, Bretz CA, Yang R, Capozzi ME, Penn JS (2014) Modulation of vegf-induced retinal vascular permeability by peroxisome proliferator-activated receptor-β/δ. Investigative Ophthalmology&Visual Science, 55:8232–8240. https://doi.org/10.1167/iovs.14-14217.
51. Klaassen I, Van Noorden CJ, Schlingemann RO (2013) Molecular basis of the inner blood-retinal barrier and its breakdown in diabetic macular edema and other pathological conditions. Progress in retinal and eye research 34:19–48. https://doi.org/10.1016/j.preteyeres.2013.02.001.
52. Maretti E, Pavan B, Rustichelli C, Montanari M, Dalpiaz A, Iannuccelli V, Leo E (2021) Chitosan/heparin polyelectrolyte complexes as ion-paring approach to encapsulate heparin in orally administrable sln: In vitro evaluation. Colloids and Surfaces A: Physicochemical and Engineering Aspects 608:125606. https://doi.org/10.1016/j.colsurfa.2020.125606
53. 53. El-Gazayerly ON, Hikal AH (1997) Preparation and evaluation of acetazolamide liposomes as an ocular delivery system. International Journal of Pharmaceutics 158:121–127. https://doi.org/10.1016/S0378-5173(97)00186-5
54. Guang W, Baraldo M, Furlanut M (1995) Calculating percentage prediction error: A user's note. Pharmacological research 32:241–248. https://doi.org/10.1016/S1043-6618(05)80029-5
55. Vilos C, Morales FA, Solar PA, Herrera NS, Gonzalez-Nilo FD, Aguayo DA, Mendoza HL, Comer J, Bravo ML, Gonzalez PA (2013) Paclitaxel-phbv nanoparticles and their toxicity to endometrial and primary ovarian cancer cells. Biomaterials 34:4098–4108. https://doi.org/10.1016/j.biomaterials.2013.02.034
56. Miller WH, Dessert AM, Roblin Jr RO (1950) Heterocyclic sulfonamides as carbonic anhydrase inhibitors. Journal of the American Chemical Society 72:4893–4896, 10.1021/ja01167a012
57. Carta F, Supuran CT, Scozzafava A (2012) Novel therapies for glaucoma: A patent review 2007–2011. Expert opinion on therapeutic patents 22:79–88. https://doi.org/10.1517/13543776.2012.649006.
58. Borhani H, Rahimy MH, Peyman GA (1994) Vitreoretinal toxicity of acetazolamide following intravitreal administration in the rabbit eye. Ophtalmic Surgery 25:166–169, PMID: 8196921
59. Galantuomo MS, Fossarello M, Cuccu A, Farci R, Preising MN, Lorenz B, Napoli PE (2016) Rebound macular edema following oral acetazolamide therapy for juvenile x-linked retinoschisis in an italian family. Clinical ophthalmology 10:2377, 10.2147/OPTH.S114568
60. Hong EH, Ahn SJ, Lim HW, Lee BR (2017) The effect of oral acetazolamide on cystoid macular edema in hydroxychloroquine retinopathy: A case report. BMC ophthalmology 17:1–5. https://doi.org/10.1186/s12886-017-0517-0

61. Jaraswekin S, Prakongpan S, Bodmeier R (2007) Effect of poly (lactide-co-glycolide) molecular weight on the release of dexamethasone sodium phosphate from microparticles. Journal of microencapsulation, 24:117–128. https://doi.org/10.1080/02652040701233655.
62. Lemarchand C, Gref R, Passirani C, Garcion E, Petri B, Müller R, Costantini D, Couvreur P (2006) Influence of polysaccharide coating on the interactions of nanoparticles with biological systems. Biomaterials 27:108–118. https://doi.org/10.1016/j.biomaterials.2005.04.041
63. Abraham SM, Lawrence T, Kleiman A, Warden P, Medghalchi M, Tuckermann J, Saklatvala J, Clark AR (2006) Antiinflammatory effects of dexamethasone are partly dependent on induction of dual specificity phosphatase 1. Journal of Experimental Medicine 203:1883–1889. https://doi.org/10.1084/jem.20060336
64. Venkatesan P, Puvvada N, Dash R, Kumar BP, Sarkar D, Azab B, Pathak A, Kundu SC, Fisher PB, Mandal M (2011) The potential of celecoxib-loaded hydroxyapatite-chitosan nanocomposite for the treatment of colon cancer. Biomaterials 32:3794–3806. https://doi.org/10.1016/j.biomaterials.2011.01.027
65. Dolati P, Khodabandeh Z, Zamiri MJ, Jamhiri I, Mehrabani D (2020) The Effect of Lead Acetate and Quercetin on the Tight and Gap Junctions in the Mouse Testis. Biological Trace Element Research 198:535–543. https://doi.org/10.1007/s12011-020-02079-x
66. Murakami T, Felinski EA, Antonetti DA (2009) Occludin phosphorylation and ubiquitination regulate tight junction trafficking and vascular endothelial growth factor-induced permeability. Journal of Biological Chemistry 284:21036–21046. https://doi.org/10.1074/jbc.M109.016766.
67. Nitta T, Hata M, Gotoh S, Seo Y, Sasaki H, Hashimoto N, Furuse M, Tsukita S (2003) Size-selective loosening of the blood-brain barrier in claudin-5–deficient mice. The Journal of cell biology 161:653–660. https://doi.org/10.1083/jcb.200302070.
68. Witmer A, Vrensen G, Van Noorden C, Schlingemann R (2003) Vascular endothelial growth factors and angiogenesis in eye disease. Progress in retinal and eye research 22:1–29. https://doi.org/10.1016/j.preteyeres.2008.05.001
69. Vinores S, Youssri A, Luna J, Chen Y, Bhargave S, Vinores M, Schoenfeld C, Peng B, Chan CC, LaRochele W, Green WR, Campochiaro PA (1997) Upregulation of vascular endothelial growth factor in ischemic and non-ischemic human and experimental retinal disease. Histology and histopathology 12:99–109, PMID: 9046048.
70. de Araújo JTC, Junior AGT, Di Filippo LD, Duarte JL, de Cássia Ribeiro T, Chorilli M (2021) Overview of chitosan-based nanosystems for prostate cancer therapy. European Polymer Journal 160:110812. https://doi.org/10.1016/j.eurpolymj.2021.110812.
71. Antonetti DA, Barber AJ, Hollinger LA, Wolpert EB, Gardner TW (1999) Vascular endothelial growth factor induces rapid phosphorylation of tight junction proteins occludin and zonula occluden 1: A potential mechanism for vascular permeability in diabetic retinopathy and tumors. Journal of Biological Chemistry 274:23463–23467. https://doi.org/10.1074/jbc.274.33.23463.
72. Harhaj NS, Felinski EA, Wolpert EB, Sundstrom JM, Gardner TW, Antonetti DA (2006) Vegf activation of protein kinase c stimulates occludin phosphorylation and contributes to endothelial permeability. Investigative Ophthalmology & Visual Science 47:5106–5115. https://doi.org/10.1167/iovs.06-0322.
73. Antonetti DA, Barber AJ, Khin S, Lieth E, Tarbell JM, Gardner TW (1998) Vascular permeability in experimental diabetes is associated with reduced endothelial occludin content: Vascular endothelial growth factor decreases occludin in retinal endothelial cells. Penn state retina research group, Diabetes, 47:1953–1959. https://doi.org/10.2337/diabetes.47.12.1953.
74. Klaassen I, Hughes JM, Vogels IM, Schalkwijk CG, Van Noorden CJ, Schlingemann RO Altered expression of genes related to blood–retina barrier disruption in streptozotocin-induced diabetes. Experimental eye research 89:4–15. https://doi.org/10.1016/j.exer.2009.01.006
75. Schlingemann RO, Hofman P, Andersson L, Troost D, van der Gaag R (1997) Vascular expression of endothelial antigen pal-e indicates absence of blood-ocular barriers in the normal eye. Ophthalmic research 29:130–138. https://doi.org/10.1159/000268007.

Figures

Figure 1

3D response surface plot demonstrating the effect of PHBV and PVA concentration on size of nanoparticles (A). 3D response surface plot demonstrating the effect of PHBV and PVA concentration on polydispersity index of nanoparticles (B). 3D response surface plot demonstrating the effect of PHBV and PVA concentration on entrapment efficiency of nanoparticles as response variable (C).

Figure 2

Nanoparticle size distribution (A) of optimized PHBV-ACZ NPs measured by dynamic light scattering (DLS). HR-SEM images of PHBV-ACZ NP (B-D) and PHBV NP (E-G) of the optimized formulation.

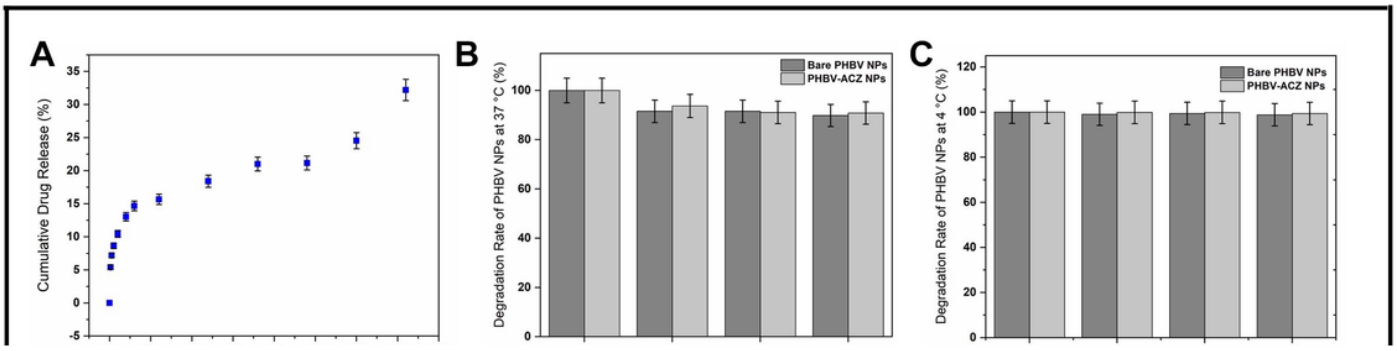

Figure 3

Release profile of ACZ from PHBV NP. in the presence of PBS, pH 7.4 (A). Degradation profiles of PHBV-NPs and ACZ-PHBV-NPs at 37°C (B) and 4°C (C)

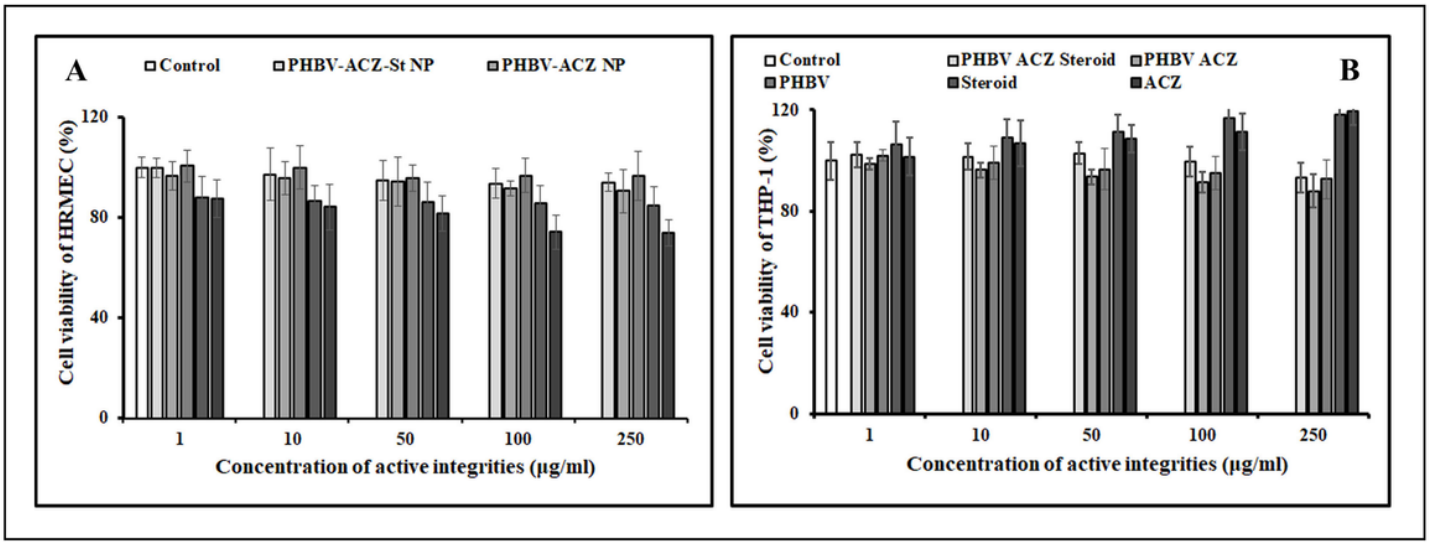

Figure 4

Cytotoxicity of different concentrations of PHBV NP, PHBV-ACZ NP, PHBV-ACZ-St NP, Steroid, and ACZ on HRMEC and THP-1 cells (n=5)

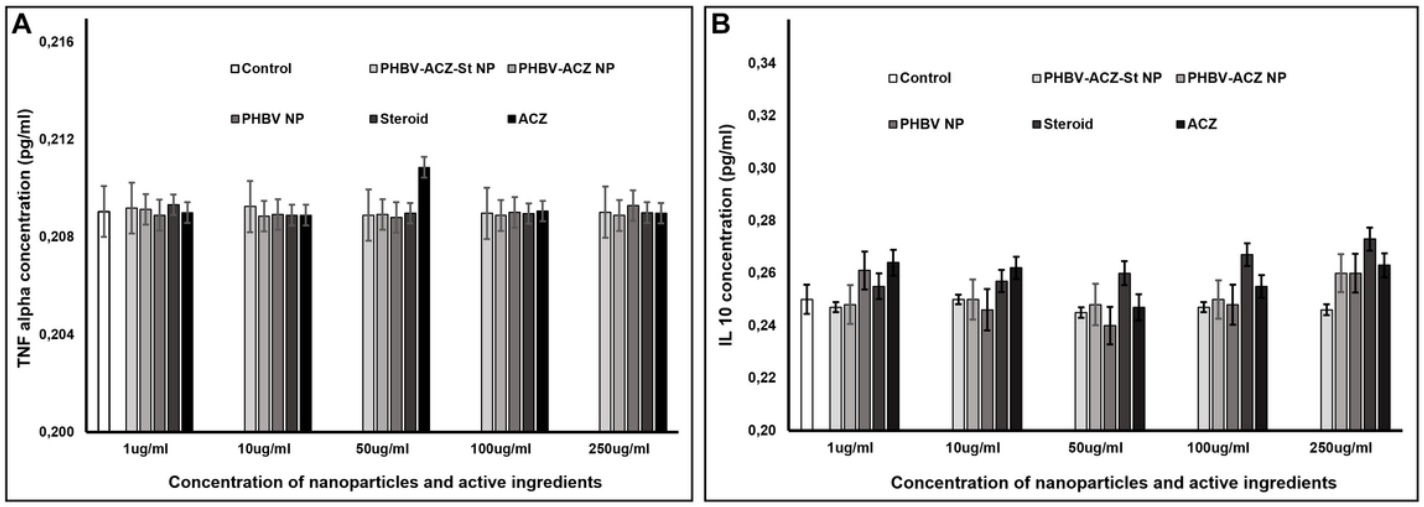

Figure 5

TNF alpha (A) and IL-10 (B) level of macrophage cells exposed to different concentrations of PHBV NP, PHBV-ACZ NP, PHBV-ACZ-St NP, Steroid, and ACZ (n=5)

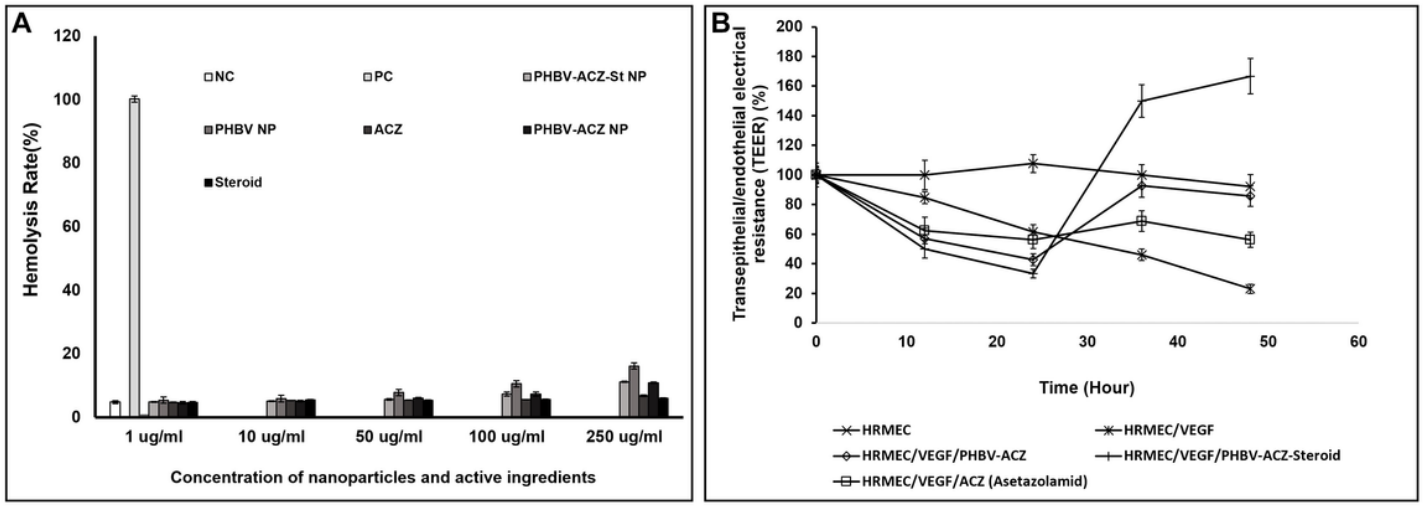

Figure 6

Hemolysis effects on red blood cell (A) and TEER value changes (B) on HRMEC exposed to different concentrations of PHBV PHBV NP, PHBV-ACZ NP, PHBV-ACZ-St NP, Steroid, and ACZ (n=3).

Figure 7

Effect of VEGF and nanoparticles on protein expression in HRMECs. Changes in expression of VE-Cad, ZO-1, claudin-5, laminin, PLVAP and Cav-1 after addition of VEGF (150 ng/ml), nanoparticles and active ingredient, as quantified by cell-based ELISA. Group 1 is HRMEC cells incubated with cell culture media. Other groups were incubated with VEGF-containing medium. Group 3 was exposed to PHBV NP, group 4 to PHBV-ACZ NP, group 5 to PHBV-ACZ-St NP, group 6 to ACZ and group 7 to steroid (n=3)